

# One-dimensional liquid ${}^4\text{He}$ : dynamical properties beyond Luttinger liquid theory

G. Bertaina,<sup>1</sup> M. Motta,<sup>2</sup> M. Rossi,<sup>3,4,5</sup> E. Vitali,<sup>2</sup> and D.E. Galli<sup>1</sup>

<sup>1</sup>*Dipartimento di Fisica, Università degli Studi di Milano, via Celoria 16, I-20133 Milano, Italy*

<sup>2</sup>*Department of Physics, The College of William and Mary, Williamsburg, Virginia 23187, USA*

<sup>3</sup>*Scuola Normale Superiore, Piazza dei Cavalieri 7, I-56126 Pisa, Italy*

<sup>4</sup>*International Center for Theoretical Physics (ICTP), Strada Costiera 11, I-34154 Trieste, Italy*

<sup>5</sup>*Dipartimento di Fisica e Astronomia, Università degli Studi di Padova, via Marzolo 8, I-35131 Padova, Italy*

We compute the zero-temperature dynamical structure factor of one-dimensional liquid  ${}^4\text{He}$  by means of state-of-the-art Quantum Monte Carlo and analytic continuation techniques. By increasing the density, the dynamical structure factor reveals a transition from a highly compressible critical liquid to a quasi-solid regime. In the low-energy limit, the dynamical structure factor can be described by the quantum hydrodynamic Luttinger liquid theory, with a Luttinger parameter spanning all possible values by increasing the density. At higher energies, our approach provides quantitative results beyond the Luttinger liquid theory. In particular, as the density increases, the interplay between dimensionality and interaction makes the dynamical structure factor manifest a pseudo *particle-hole* continuum typical of fermionic systems. At the low-energy boundary of such region and moderate densities, we find consistency, within statistical uncertainties, with predictions of a power-law structure by the recently-developed non-linear Luttinger liquid theory. In the quasi-solid regime we observe a novel behavior at intermediate momenta, which can be described by new analytical relations that we derive for the hard-rods model.

One-dimensional (1D) quantum systems exhibit some of the most diverse and fascinating phenomena of condensed matter Physics [1–3]. Among the most spectacular signatures of the interplay between quantum fluctuations, interaction and reduced dimensionality, are the breakdown of ordered phases in presence of short-range interactions [4], and the loosened distinction between Bose and Fermi behavior [5]. The study of quasi-1D quantum systems is a very active research field, aroused by the experimental investigation of electronic transport properties [6–10], by the fabrication of long 1D arrays of Josephson junctions [11], and recently corroborated by the availability of ultracold atomic gases in highly anisotropic traps and optical lattices [2, 12–14], as well as by experiments on confined He atoms [15–19].

The low-energy properties of a wide class of Bose and Fermi 1D quantum systems [1, 20] are notoriously captured by the phenomenological Tomonaga-Luttinger liquid (TLL) theory [21–23], characterized by collective phonon-like excitations. This theory introduces two conjugate Bose fields  $\phi(x)$ ,  $\theta(x)$  describing, respectively, the density and phase fluctuations of the field operator  $\psi(x) = \sqrt{\rho + \partial_x \phi(x)} e^{i\theta(x)}$ , where  $\rho$  is the average density. Those fields are described by the exactly-solvable low-energy effective Hamiltonian:

$$H_{LL} = \frac{\hbar}{2\pi} \int dx \left( cK_L \partial_x \theta(x)^2 + \frac{c}{K_L} \partial_x \phi(x)^2 \right) . \quad (1)$$

Although in general the TLL parameter  $K_L$  and the sound velocity  $c$  are independent quantities (notably in lattice models), for Galilean-invariant systems  $c = \frac{v_F}{K_L}$  [23],  $v_F = \frac{\hbar k_F}{m}$  being the Fermi velocity and  $k_F = \pi \rho$  the Fermi wavevector of a 1D ideal Fermi gas (IFG), and  $K_L$  is thus related to the compressibility  $\kappa_S$  by

$m K_L^2 = \hbar^2 \pi^2 \rho^3 \kappa_S$ . Such collective excitations are revealed by the low-momentum and low-energy behavior of the dynamical structure factor:

$$S(q, \omega) = \int dt \frac{e^{i\omega t}}{2\pi N} \langle e^{\frac{iH}{\hbar}} \rho_q e^{-\frac{iH}{\hbar}} \rho_{-q} \rangle , \quad (2)$$

where  $\rho_q = \sum_{i=1}^N e^{iqx_i}$  is the Fourier transform of the density operator,  $N$  the number of particles,  $H$  the Hamiltonian and  $x_i$  the position of the  $i$ -th particle [24]. A complete characterization of density fluctuations requires to compute (2) also beyond the limits of applicability of TLL theory. A deep insight in the characterization of (2) at higher frequencies is provided by the phenomenological nonlinear TLL theory [3, 25]; for integrable models, quantitative results are also provided by nonperturbative numeric calculations [13, 14, 26–28]. For physically-relevant non-integrable systems, on the other hand, the study of (2) requires more general approaches.

In this Letter, we probe the excitations of 1D liquid  ${}^4\text{He}$  by evaluating its complete zero-temperature dynamical structure factor with fully *ab-initio* methods. When strictly confined in 1D,  ${}^4\text{He}$  provides a spectacular condensed-matter realization of a TLL, having the unique feature of spanning all possible values of  $K_L$  by only varying the density. The interest in this system emerges also in connection with experimental realizations and theoretical characterizations of quasi-1D He systems confined inside nanopores [17, 29–31] or moving inside dislocation lines in crystalline He samples [18, 19, 32]. A realistic microscopic description of the system is provided by the Hamiltonian:

$$H = -\frac{\hbar^2}{2m} \sum_{i=1}^N \frac{\partial^2}{\partial x_i^2} + \sum_{i < j=1}^N V(x_i - x_j) , \quad (3)$$

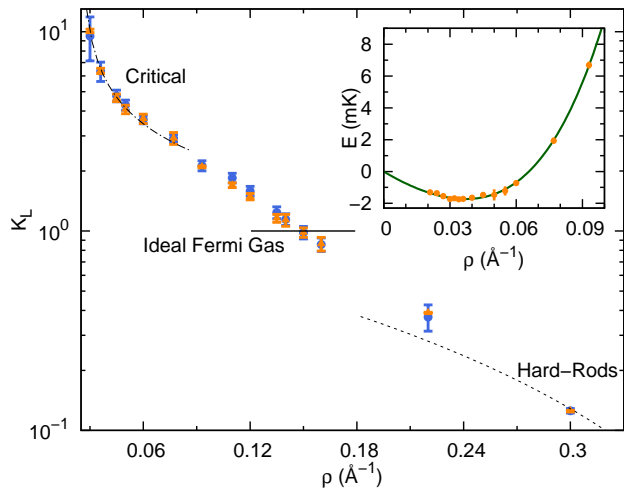


Figure 1. (color online) TLL parameter  $K_L$ , from the compressibility  $\kappa_S^{-1} = \rho \partial_\rho (\rho^2 \partial_\rho E(\rho))$  (blue circles) and the low- $q$  behavior of  $S(q)$  (orange triangles). Superimposed lines are described in the text. Inset: equation of state  $E(\rho)$ .

$V(x)$  being the well-established Aziz potential [33]. We access  $S(q, \omega)$  by performing an inverse Laplace transform of the imaginary-time correlation function:

$$F(q, \tau) = \frac{1}{N} \langle e^{\frac{\tau H}{\hbar}} \rho_q e^{-\frac{\tau H}{\hbar}} \rho_{-q} \rangle = \int_0^\infty d\omega e^{-\tau \omega} S(q, \omega). \quad (4)$$

We compute  $F(q, \tau)$  using the Path Integral Ground State (PIGS) method [34, 35], which provides unbiased [36] estimates of ground-state properties and imaginary-time correlations by statistically sampling the wavefunction  $\Psi_\tau = e^{-\tau H} \Psi_T$ , where  $\Psi_T$  is a trial state [37, 38], non-orthogonal to the ground state of  $H$ . At sufficiently large  $\tau$ , the expectation values over  $\Psi_\tau$  are compatible with ground-state averages. We simulate up to  $N = 160$  particles using periodic boundary conditions and find that our results are representative of the thermodynamic limit already for  $N = 40$  particles within statistical uncertainty (see Supplemental Material [39]). Inverting the Laplace transform in Eq. (4) is notoriously an ill-posed inverse problem, meaning that many possible  $S(q, \omega)$  are compatible with the imaginary-time data. However, a number of inversion strategies have provided reliable results for physically relevant systems [40–43]. In this Letter, we use the state-of-the-art Genetic Inversion via Falsification of Theories (GIFT) algorithm [43–50].

We study the Galilean-invariant liquid phase which is notoriously stable above the density  $\rho_{sp} = 0.026(2) \text{ \AA}^{-1}$ , where it undergoes a spinodal decomposition [51–53], namely the formation of liquid droplets. In Fig. 1, we compute the TLL parameter  $K_L$  of the system as a function of  $\rho > \rho_{sp}$  from both the compressibility and the sound velocity, inferred from the low-momentum behavior of the static structure factor  $S(q) = F(q, 0) \simeq K_L \frac{q}{2k_F}$ . The good agreement between the two estimates over the whole density range confirms their accuracy, and the in-

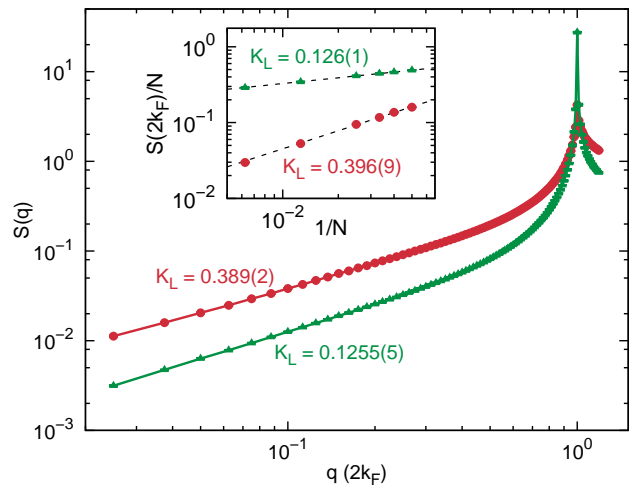


Figure 2. (color online) Static structure factor  $S(q)$  at  $\rho = 0.22, 0.30 \text{ \AA}^{-1}$  (red circles, green triangles). Inset: Scaling of  $S(2k_F)$  with  $N$  at the same densities (dashed lines: fit to a power-law). Values of  $K_L$  from  $c$  and the scaling of  $S(2k_F)$  are reported.

ternal consistency of our approach. Close to the spinodal decomposition, the sound velocity provides a more precise estimate of  $K_L$  [54]. As the density increases,  $K_L$  monotonically decreases from  $\infty$  to 0, manifesting three fundamental regimes. At density  $\rho \lesssim 0.06 \text{ \AA}^{-1}$  the system is in the spinodal critical regime and we observe  $K_L \propto (\rho - \rho_{sp})^{-\zeta}$  with  $\zeta \simeq 0.5$ . This is equivalent to a dependence  $c \propto (P - P_{sp})^\nu$  of sound velocity with the pressure difference  $P - P_{sp}$ , with  $P_{sp}$  the pressure at the spinodal point and  $\nu = \zeta / (2\zeta + 1) \simeq 0.25$ , which is interestingly consistent with the critical value in three-dimensional helium [55–58]. At density  $\rho \gtrsim 0.30 \text{ \AA}^{-1}$  we observe instead a good agreement with the hard-rods (HR) model [59], defined by  $V(x) = \infty$  for  $|x| < a$  and 0 otherwise. In Fig. 1 we take  $a = 2.139 \text{ \AA}$ , which is the scattering length of the repulsive part of the  $^4\text{He}$  potential as in [60]. The HR model spans all values of  $K_L = (1 - \rho a)^2 < 1$  as a function of the density. At the intermediate density  $\rho \simeq 0.150 \text{ \AA}^{-1}$   $^4\text{He}$  attains  $K_L = 1$ , which is the TLL parameter of the Tonks-Girardeau gas of impenetrable point-like Bosons [5] and of the 1D IFG.

The diverse behavior of  $^4\text{He}$  is a peculiar consequence of the interplay between the hard-core repulsion and the Van der Waals attraction in the interaction potential, and the mass of the atoms. It has been recently recognized that the TLL parameter of  $^3\text{He}$  features a similar high-density behavior [61]; the low-density behavior, however, is remarkably different as the smaller mass of  $^3\text{He}$  prevents a spinodal decomposition, maintaining  $K_L$  and the compressibility below a finite value.

In view of the universality of TLL theory, knowledge of  $K_L$  sheds light on the low-momentum and low-energy structure of  $S(q, \omega)$ . TLL theory also predicts [62–64] a power-law singularity  $S(q = 2k_{Fj}, \omega) \sim \omega^{2(j^2 K_L - 1)}$  for

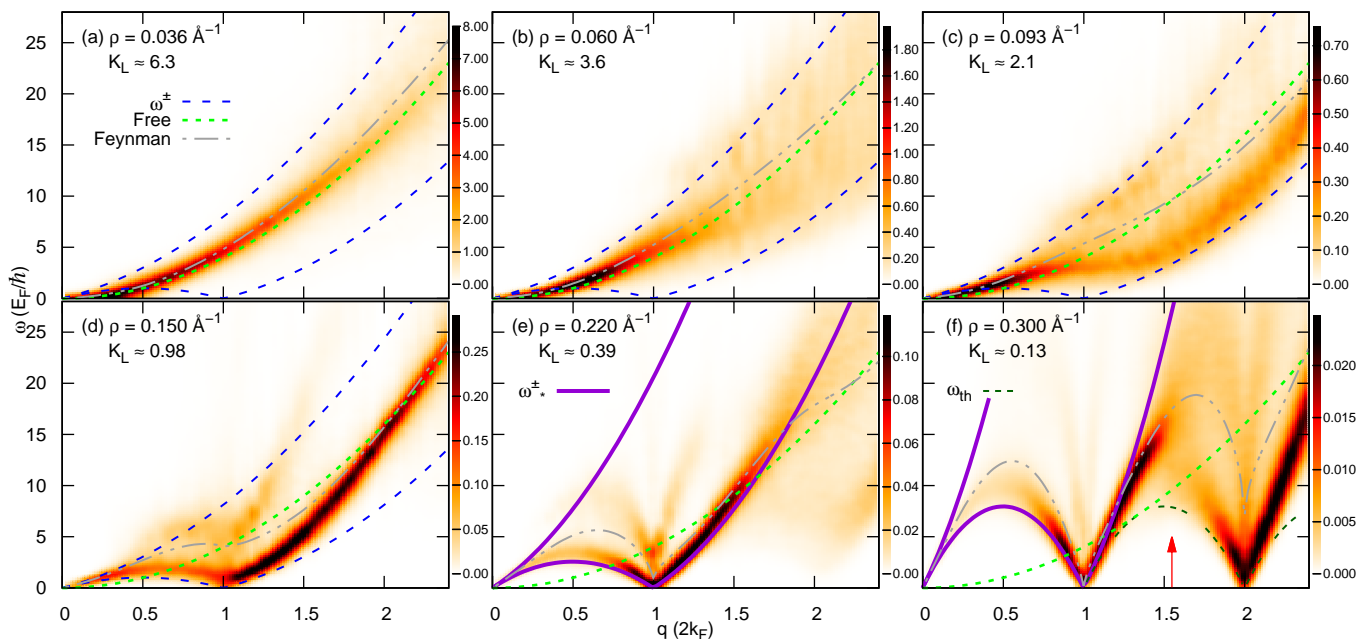


Figure 3. (color online) Color plot of  $S(q, \omega)$  at several densities and corresponding  $K_L$ . Feynman approximation  $\omega_F(q)$  (gray dash-dotted lines) and the free particle dispersion  $\hbar q^2/2m$  (green dotted lines) are drawn for comparison. Panels (a-d) show also the bounds  $\omega^\pm(q)$  of the particle-hole band (blue dashed line), while panels (e-f) show the bounds  $\omega_\pm^*(q)$  of the HR elementary excitations (violet solid line). Panel (f) shows the low-energy threshold  $\omega_{\text{th}}(q)$  of HR with  $K_L = 0.125$  (double-dashed line), and momentum  $Q_1$  (red arrow). Values of  $S(q, \omega)$  beyond scale are plot in black.

$\omega \rightarrow 0$  and integer ( $j \in \mathbb{N}$ ) multiples of  $2k_F$ . Such singularity is strictly related to the emergence of quasi-Bragg peaks in the static structure factor, featuring a sub-linear growth  $S(2k_F j) \propto N^{1-2j^2 K_L}$  [59] with the number of particles. The height of the  $j$ -th peak diverges, in the thermodynamic limit, provided that  $2j^2 K_L < 1$ . In Fig. 2 we observe the emergence of quasi-Bragg peaks in  $S(2k_F)$  at densities  $\rho > 0.196(5) \text{ \AA}^{-1}$ , where  $K_L < 1/2$ . This is naturally expected since the small compressibility sets up a diagonal quasi-long range order, while crystallization is prohibited by the dimensionality and by the range of the interaction [59]. The scaling of  $S(2k_F)$  with  $N$ , reported in the inset of Fig. 2, provides an alternative estimate of  $K_L$ , in agreement with the results in Fig. 1.

The rich physical behavior suggested by the TLL parameter is notably unveiled by the dynamical structure factor, that our approach characterizes over the entire momentum-energy plane. Fig. 3 shows  $S(q, \omega)$  as a function of momentum and frequency, in Fermi units  $2k_F$  and  $E_F/\hbar = \hbar k_F^2/2m$  respectively, at several representative densities. We show also Feynman's approximation for the excitation spectrum  $\omega_F(q) = \hbar q^2/2m S(q)$ , which postulates a single mode saturating the f-sum rule  $\hbar q^2/2m = \int d\omega S(q, \omega) \omega$ . Departures from the Feynman spectrum indicate a broadening or the presence of multiple modes [65].

As expected, for small  $q$  and  $\omega$ ,  $S(q, \omega)$  is always peaked around the phonon dispersion relation  $\omega = cq$ .

On the other hand, the high-energy scenario is strikingly different and strongly dependent on the density. At  $K_L \simeq 6.3$  (Fig. 3a) the spectral weight is very close to the free particle dispersion, consistently with similar predictions for 3D helium at negative pressures [55–58]. Such behavior is common to the Lieb-Liniger contact interaction model at large  $K_L$  [26, 66, 67], although in the case of  $^4\text{He}$  the physical origin of such a behavior lies in the spinodal critical point. At large momentum ( $q \gtrsim k_F$ ) and energy we observe a broadening of  $S(q, \omega)$ , that makes more and more pronounced as  $K_L$  decreases (Fig. 3b,c). As in the Lieb-Liniger model [26], the spectral weight of  $S(q, \omega)$  partially fills the particle-hole band of the 1D IFG, enclosed between the dispersion relations  $\omega^\pm(q) = |v_F q \pm \hbar q^2/2m|$ . In both cases, this reveals a tendency for fermionization [5]: the repulsive interaction between 1D bosons mimics the Pauli exclusion principle, and makes  $S(q, \omega)$  manifest the particle-hole continuum typical of spinless free fermions. At  $K_L \simeq 2.1$  (Fig. 3c) the spectral weight of  $^4\text{He}$  starts to concentrate again, emerging as a phonon and then bending downwards to approach  $\omega^-(q)$ . Such peculiar behavior is reminiscent of the deflection of the Bogoliubov mode in 3D systems of hard spheres [50, 68], with the notable difference that in 1D the spectral weight at  $q \simeq 2k_F j$  is non-zero up to very low frequency. At  $K_L \simeq 1$  (Fig. 3d) the incipient concentration of the spectral weight makes strikingly manifest and takes place around a low-energy excitation, which

is close to  $\omega^-(q)$  for  $q < 2k_F$  and approaches the free particle dispersion relation for higher momentum. However,  $S(2k_F, \omega)$  is almost flat at low frequency  $\omega \lesssim E_F/\hbar$ , within our resolution (see Supplemental Material [39]), analogously to the Tonks-Girardeau and IFG models. Above the low-energy excitation a lower-intensity secondary structure overhangs; for  $K_L < 1$  (Fig. 3e,f) it evolves into a well-defined high-energy structure attaining a non-zero local minimum at  $q = 2k_F$ , in correspondence of the free-particle energy. Although a precise characterization of this structure requires further investigation, it is reminiscent of a 3D rotonic behavior or of multi-phonons [50, 68–70]. For  $K_L \simeq 0.39$  (Fig. 3e)  $S(q, \omega)$  is mostly distributed in a region with boundaries  $\omega_*^\pm(q)$ , which are modified with respect to  $\omega^\pm(q)$  as an effect of interaction, and the spectral weight concentrates close to the lower branch  $\omega_*^-(q)$ . We notice that  $\omega_*^\pm(q) = \omega^\pm(q)/K_L$  (solid lines in Fig. 3e,f). A similar behavior can be discerned [71] in the Super Tonks-Girardeau gas [72, 73], a gaseous excited state of the attractive Lieb-Liniger model. This behavior can be quantitatively explained: in the high-density regime the main interaction effect is volume exclusion, as in the HR model. The solution of such model via the Bethe Ansatz technique [74–76] shows that the eigenfunctions of the HR Hamiltonian can be mapped onto those of an IFG with increased density  $\rho/(1-\rho a)$ , thus yielding a scaling factor  $(1-\rho a)^{-2} = K_L^{-1}$  in the boundaries of the particle-hole band.

The distribution of spectral weight changes dramatically for  $K_L \simeq 0.125$  (Fig. 3f) for  $2k_F < q < 4k_F$ , where the low-energy excitation rapidly broadens and flattens at  $q \simeq 3.2k_F$ , and concentrates again at a lower energy around  $q \simeq 4k_F$ . A quantitative explanation of this effect can be given in the light of the recently-developed nonlinear TLL theory [3], again modeling  $^4\text{He}$  atoms with HR. Nonlinear TLL theory assumes the existence of a low-energy threshold  $\omega_{\text{th}}(q)$ , below which no excitations are present. Interpreting an excitation with frequency  $\omega \gtrsim \omega_{\text{th}}(q)$  as the creation of a mobile impurity in an otherwise usual TLL, nonlinear TLL theory shows that  $S(q, \omega)$  features a power-law singularity:

$$S(q, \omega) \propto \Theta(\omega - \omega_{\text{th}}(q)) |\omega - \omega_{\text{th}}(q)|^{-\lambda(q)}, \quad (5)$$

where  $\lambda(q)$  is a function of  $K_L$  and  $\omega_{\text{th}}(q)$  [25] and  $\Theta(\omega)$  is the Heaviside step function. The expansion  $\omega_{\text{th}}(q) \approx cq - \hbar q^2/2m^*$  of the low-energy threshold around  $q = 0$  defines the effective mass  $m^*$ , which sets the energy scale where modifications from TLL theory take place [25]. The effective mass is a function  $1/m^* = c \partial_\mu (c\sqrt{K_L})/K_L$  of  $K_L$  and the chemical potential  $\mu$  [25, 77]. For the HR model we indeed derive  $m/m^* = 1/K_L$ , indicating that  $\omega_{\text{th}}(q) \approx \omega_*^-(q)$  for small momentum. This is again confirmed over the whole range  $0 \leq q \leq 2k_F$  by the analytical solution of the HR model [76]. Away from this basic region, the

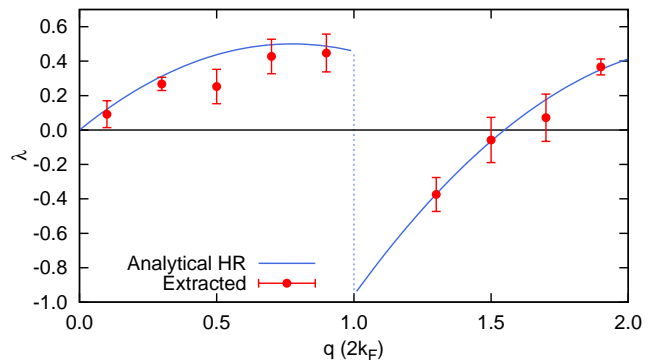


Figure 4. (color online) Analytical non-linear TLL exponent Eq. (6) for HR with  $K_L = 0.125$  (solid line) and PIGS+GIFT (circles) fitted exponents of  $^4\text{He}$  at density  $\rho = 0.3\text{\AA}^{-1}$ .

low-energy threshold repeats periodically [3, 63, 78] as shown in Fig. 3f: therefore  $\omega_{\text{th}}(q) = \omega_*^-(q - 2nk_F)$  with  $2nk_F < q < 2(n+1)k_F$  and  $n$  integer.

For the HR model, given the analytic expressions of  $K_L$  and  $\omega_{\text{th}}(q)$ , we extract the exponents following [25]:

$$\lambda(q) = -2(\tilde{q} - n)(\tilde{q} - n - 1), \quad \tilde{q} \equiv qa/2\pi. \quad (6)$$

In Fig. 4 we show  $\lambda(q)$  for a HR system with the same  $K_L$  as in Fig. 3f, comparing it to numerically extracted exponents as described below.  $\lambda(q)$  is a piecewise continuous function of  $q$ , with jump singularities at  $q = 2nk_F$ . For  $0 \leq q < 2k_F$ ,  $\lambda(q) > 0$  and  $S(q, \omega)$  diverges close to  $\omega_{\text{th}}(q)$ . After  $q = 2k_F$ ,  $\lambda(q)$  changes sign and thus  $S(q, \omega)$  vanishes close to  $\omega_{\text{th}}(q)$ . In fact, for  $2k_F < q \lesssim 3.2k_F$ , the spectral weight concentrates much above  $\omega_{\text{th}}(q)$ , around  $\omega_*^-(q)$ , a feature which is even beyond nonlinear TLL theory. Eq. (6) predicts a flat  $S(q, \omega)$  at the special wavevectors  $Q_n = 2\pi n/a$ , consistently with a previous result [59] based on exact properties of the HR model. We indeed observe almost flat  $S(q, \omega)$  at  $Q_1 = 3.24k_F \simeq 2\pi/a$  (red arrow in Fig. 3f). Beyond  $Q_1$  the divergence reappears, since  $\lambda(q) < 0$ .

To quantitatively verify prediction (6), for some momenta we have performed much more refined reconstructions at  $\rho = 0.3\text{\AA}^{-1}$ , imposing  $S(q, \omega) = 0$  [79] below the exact  $\omega_{\text{th}}(q)$  for the HR model, and fitting the obtained spectrum to a power law (see Supplemental Material [39]). The obtained exponents are indicated in Fig. 4: this procedure does not disprove the power-law model (5) in a range of frequencies up to  $\sim \omega_{\text{th}}(q) + E_F/\hbar$ , depending on momentum [80], and yields exponents  $\lambda(q)$  which are consistent with the nonlinear TLL prediction (6) within statistical uncertainty. This result is quite remarkable, since no prior knowledge about  $S(q, \omega)$  has been enforced in the analytic continuations, except for the f-sum rule and the exact threshold for HR [81].

We have thus provided a robust description of the system in the experimentally-relevant high-density regime, based on the HR model, which almost fully characterizes the spectrum at low and intermediate energies. The novel

structure predicted around momenta that are multiples of  $2\pi/a$  is relevant, and would be very interesting to experimentally observe, for all quantum excluded-volume systems, such as liquid He inside nanopores, Rydberg gases [82, 83] and Super-Tonks-Girardeau gases.

We acknowledge very useful discussions with G. Astrakharchik. We are grateful to A. Parola for revising the manuscript. We thank M. Panfil and co-authors for providing us with their data on the Super-Tonks-Girardeau gas. The simulations were performed on the supercomputing facilities at CINECA and at the Physics Departments of the Universities of Milan and Padua. We thank the Computing Support Staff at INFN and Physics Department of the University of Milan. We acknowledge the CINECA and the Regione Lombardia award LI03p-UltraQMC, under the LISA initiative, for the availability of high-performance computing resources and support. M.M. acknowledges funding from the Dr. Davide Colosimo Award, celebrating the memory of physicist Davide Colosimo. M.M. and E.V. acknowledge support from the Physics Department of the University of Milan, the Simons Foundation and NSF (Grant no. DMR-1409510). G.B. and D.E.G. acknowledge funding from D.E. Pini.

- 
- [1] T. Giamarchi, *Quantum Physics in One Dimension* (Oxford University Press, 2003).
- [2] M. A. Cazalilla, R. Citro, T. Giamarchi, E. Orignac, and M. Rigol, “One dimensional bosons: From condensed matter systems to ultracold gases,” *Rev. Mod. Phys.* **83**, 1405–1466 (2011).
- [3] A. Imambekov, T. L. Schmidt, and L. I. Glazman, “One-dimensional quantum liquids: Beyond the Luttinger liquid paradigm,” *Rev. Mod. Phys.* **84**, 1253–1306 (2012).
- [4] N. D. Mermin and H. Wagner, “Absence of Ferromagnetism or Antiferromagnetism in One- or Two-Dimensional Isotropic Heisenberg Models,” *Phys. Rev. Lett.* **17**, 1133–1136 (1966).
- [5] M. Girardeau, “Relationship between Systems of Impenetrable Bosons and Fermions in One Dimension,” *J. Math. Phys.* **1**, 516–523 (1960).
- [6] A. M. Chang, L. N. Pfeiffer, and K. W. West, “Observation of Chiral Luttinger Behavior in Electron Tunneling into Fractional Quantum Hall Edges,” *Phys. Rev. Lett.* **77**, 2538–2541 (1996).
- [7] Z. Yao, H. W. Ch. Postma, L. Balents, and C. Dekker, “Carbon nanotube intramolecular junctions,” *Nature* **402**, 273–276 (1999).
- [8] M. Bockrath, D. H. Cobden, J. Lu, A. G. Rinzler, R. E. Smalley, L. Balents, and P. L. McEuen, “Luttinger-liquid behaviour in carbon nanotubes,” *Nature* **397**, 598–601 (1999).
- [9] A. N. Aleshin, H. J. Lee, Y. W. Park, and K. Akagi, “One-Dimensional Transport in Polymer Nanofibers,” *Phys. Rev. Lett.* **93**, 196601 (2004).
- [10] S. V. Zaitsev-Zotov, Y. A. Kumzerov, Y. A. Firsov, and P. Monceau, “Luttinger-liquid-like transport in long InSb nanowires,” *Journal of Physics: Condensed Matter* **12**, L303 (2000).
- [11] E. Chow, P. Delsing, and D. B. Haviland, “Length-Scale Dependence of the Superconductor-to-Insulator Quantum Phase Transition in One Dimension,” *Phys. Rev. Lett.* **81**, 204–207 (1998).
- [12] I. Bloch and W. Zwerger, “Many-body physics with ultracold gases,” *Rev. Mod. Phys.* **80**, 885–964 (2008).
- [13] N. Fabbri, M. Panfil, D. Clément, L. Fallani, M. Inguscio, C. Fort, and J.-S. Caux, “Dynamical structure factor of one-dimensional Bose gases: Experimental signatures of beyond-Luttinger-liquid physics,” *Phys. Rev. A* **91**, 043617 (2015).
- [14] F. Meinert, M. Panfil, M. J. Mark, K. Lauber, J.-S. Caux, and H.-C. Nägerl, “Probing the Excitations of a Lieb-Liniger Gas from Weak to Strong Coupling,” *Phys. Rev. Lett.* **115**, 085301 (2015).
- [15] B. Yager, J. Nyéki, A. Casey, B. P. Cowan, C. P. Lusher, and J. Saunders, “NMR Signature of One-Dimensional Behavior of  $^3\text{He}$  in Nanopores,” *Phys. Rev. Lett.* **111**, 215303 (2013).
- [16] M. Savard, G. Dauphinais, and G. Gervais, “Hydrodynamics of Superfluid Helium in a Single Nanohole,” *Phys. Rev. Lett.* **107**, 254501 (2011).
- [17] J. Taniguchi, K. Demura, and M. Suzuki, “Dynamical superfluid response of  $^4\text{He}$  confined in a nanometer-size channel,” *Phys. Rev. B* **88**, 014502 (2013).
- [18] Y. Vekhov and R. B. Hallock, “Mass Flux Characteristics in Solid  $^4\text{He}$  for  $T > 100$  mK: Evidence for Bosonic Luttinger-Liquid Behavior,” *Phys. Rev. Lett.* **109**, 045303 (2012).
- [19] Ye. Vekhov and R. B. Hallock, “Dissipative superfluid mass flux through solid  $^4\text{He}$ ,” *Phys. Rev. B* **90**, 134511 (2014).
- [20] G. F. Giuliani and G. Vignale, *Quantum Theory of the Electron Liquid* (Cambridge University Press, 2005).
- [21] Tomonaga, S.-I., “Remarks on Bloch’s Method of Sound Waves applied to Many-Fermion Problems,” *Prog. Theor. Phys.* **5**, 544 (1950).
- [22] J. M. Luttinger, “An Exactly Soluble Model of a Many-Fermion System,” *J. Math. Phys.* **4**, 1154–1162 (1963).
- [23] F. D. M. Haldane, “Effective Harmonic-Fluid Approach to Low-Energy Properties of One-Dimensional Quantum Fluids,” *Phys. Rev. Lett.* **47**, 1840–1843 (1981).
- [24] Such quantity is related to the imaginary part of the density-density response function by the fluctuation-dissipation theorem. See R. Kubo, “The fluctuation-dissipation theorem,” *Rep. Prog. Phys.* **29**, 255–284 (1966).
- [25] A. Imambekov and L. I. Glazman, “Phenomenology of One-Dimensional Quantum Liquids Beyond the Low-Energy Limit,” *Phys. Rev. Lett.* **102**, 126405 (2009).
- [26] J.-S. Caux and P. Calabrese, “Dynamical density-density correlations in the one-dimensional Bose gas,” *Phys. Rev. A* **74**, 031605 (2006).
- [27] M. Mourigal, M. Enderle, A. Klöpperpieper, J.-S. Caux, A. Stunault, and H. M. Rønnow, “Fractional spinon excitations in the quantum Heisenberg antiferromagnetic chain,” *Nat. Phys.* **9**, 435–441 (2013).
- [28] B. Lake, D. A. Tennant, J.-S. Caux, T. Barthel, U. Schollwöck, S. E. Nagler, and C. D. Frost, “Multispinon Continua at Zero and Finite Temperature in a Near-Ideal Heisenberg Chain,” *Phys. Rev. Lett.* **111**,

- 137205 (2013).
- [29] C. T. Kresge, M. E. Leonowicz, W. J. Roth, J. C. Vartuli, and J. S. Beck, "Ordered mesoporous molecular sieves synthesized by a liquid-crystal template mechanism," *Nature* **359**, 710–712 (1992).
- [30] A. Del Maestro and I. Affleck, "Interacting bosons in one dimension and the applicability of Luttinger-liquid theory as revealed by path-integral quantum Monte Carlo calculations," *Phys. Rev. B* **82**, 060515 (2010).
- [31] A. Del Maestro, M. Boninsegni, and I. Affleck, "<sup>4</sup>He Luttinger Liquid in Nanopores," *Phys. Rev. Lett.* **106**, 105303 (2011).
- [32] M. Boninsegni, A. B. Kuklov, L. Pollet, N. V. Prokof'ev, B. V. Svistunov, and M. Troyer, "Luttinger Liquid in the Core of a Screw Dislocation in Helium-4," *Phys. Rev. Lett.* **99**, 035301 (2007).
- [33] R. A. Aziz, V. P. S. Nain, J. S. Carley, W. L. Taylor, and G. T. McConville, "An accurate intermolecular potential for helium," *The Journal of Chemical Physics* **70**, 4330–4342 (1979).
- [34] A. Sarsa, K. E. Schmidt, and W. R. Magro, "A path integral ground state method," *The Journal of Chemical Physics* **113**, 1366–1371 (2000).
- [35] D. E. Galli and L. Reatto, "Recent progress in simulation of the ground state of many Boson systems," *Molecular Physics* **101**, 1697–1703 (2003).
- [36] M. Rossi, M. Nava, L. Reatto, and D. E. Galli, "Exact ground state Monte Carlo method for Bosons without importance sampling," *J. Chem. Phys.* **131**, 154108 (2009).
- [37] L. Reatto and G. V. Chester, "Phonons and the Properties of a Bose System," *Phys. Rev.* **155**, 88–100 (1967).
- [38] S. Vitiello, K. Runge, and M. H. Kalos, "Variational Calculations for Solid and Liquid <sup>4</sup>He with a "Shadow" Wave Function," *Phys. Rev. Lett.* **60**, 1970–1972 (1988).
- [39] See Supplemental Material at *url* for details on the PIGS and GIFT methods and examples of fits of the spectra at given momenta.
- [40] A. W. Sandvik, "Stochastic method for analytic continuation of quantum Monte Carlo data," *Phys. Rev. B* **57**, 10287–10290 (1998).
- [41] A. S. Mishchenko, N. V. Prokof'ev, A. Sakamoto, and B. V. Svistunov, "Diagrammatic quantum Monte Carlo study of the Fröhlich polaron," *Phys. Rev. B* **62**, 6317–6336 (2000).
- [42] D. R. Reichman and E. Rabani, "Analytic continuation average spectrum method for quantum liquids," *J. Chem. Phys.* **131**, 054502 (2009).
- [43] Vitali, E. and Rossi, M. and Reatto, L. and Galli, D. E., "Ab initio low-energy dynamics of superfluid and solid <sup>4</sup>He," *Phys. Rev. B* **82**, 174510 (2010).
- [44] M. Rossi, E. Vitali, L. Reatto, and D. E. Galli, "Microscopic characterization of overpressurized superfluid <sup>4</sup>He," *Phys. Rev. B* **85**, 014525 (2012).
- [45] S. Sacconi, S. Moroni, E. Vitali, and M. Boninsegni, "Bose soft discs: a minimal model for supersolidity," *Mol. Phys.* **109**, 2807–2812 (2011).
- [46] S. Sacconi, S. Moroni, and M. Boninsegni, "Excitation Spectrum of a Supersolid," *Phys. Rev. Lett.* **108**, 175301 (2012).
- [47] M. Nava, D. E. Galli, M. W. Cole, and L. Reatto, "Superfluid State of <sup>4</sup>He on Graphane and Graphene-Fluoride: Anisotropic Roton States," *J Low Temp Phys* **171**, 699–710 (2012).
- [48] M. Nava, D. E. Galli, S. Moroni, and E. Vitali, "Dynamic structure factor for <sup>3</sup>He in two dimensions," *Phys. Rev. B* **87**, 144506 (2013).
- [49] F. Arrigoni, E. Vitali, D. E. Galli, and L. Reatto, "Excitation spectrum in two-dimensional superfluid <sup>4</sup>He," *Low Temp. Phys.* **39**, 793–800 (2013).
- [50] R. Rota, F. Tramonto, D. E. Galli, and S. Giorgini, "Quantum Monte Carlo study of the dynamic structure factor in the gas and crystal phase of hard-sphere bosons," *Phys. Rev. B* **88**, 214505 (2013).
- [51] G. Stan, V. H. Crespi, M. W. Cole, and M. Boninsegni, "Interstitial He and Ne in Nanotube Bundles," *J. Low Temp. Phys.* **113**, 447–452 (1998).
- [52] E. Krotscheck and M. D. Miller, "Properties of <sup>4</sup>He in one dimension," *Phys. Rev. B* **60**, 13038–13050 (1999).
- [53] M. Boninsegni and S. Moroni, "Ground State of <sup>4</sup>He in One Dimension," *J. Low Temp. Phys.* **118**, 1–6 (2000).
- [54] Estimating  $K_L$  from  $\kappa_S$  requires differentiation of the equation of state, which is fitted to a polynomial. Uncertainties on the fit parameters propagate to  $\kappa_S$ , resulting in unavoidably large error bars near the spinodal decomposition, where the compressibility diverges.
- [55] F. Albergamo, J. Bossy, P. Averbuch, H. Schober, and H. R. Glyde, "Phonon-Roton Excitations in Liquid <sup>4</sup>He at Negative Pressures," *Phys. Rev. Lett.* **92**, 235301 (2004).
- [56] M. A. Solís and J. Navarro, "Liquid <sup>4</sup>He and <sup>3</sup>He at negative pressure," *Phys. Rev. B* **45**, 13080–13083 (1992).
- [57] J. Boronat, J. Casulleras, and J. Navarro, "Monte Carlo calculations for liquid <sup>4</sup>He at negative pressure," *Phys. Rev. B* **50**, 3427–3430 (1994).
- [58] G. H. Bauer, D. M. Ceperley, and N. Goldenfeld, "Path-integral Monte Carlo simulation of helium at negative pressures," *Phys. Rev. B* **61**, 9055–9060 (2000).
- [59] F. Mazzanti, G. E. Astrakharchik, J. Boronat, and J. Casulleras, "Ground-State Properties of a One-Dimensional System of Hard Rods," *Phys. Rev. Lett.* **100**, 020401 (2008).
- [60] See M. Kalos, D. Levesque, and L. Verlet, "Helium at zero temperature with hard-sphere and other forces," *Phys. Rev. A* **9**, 2178–2195 (1974). Note that due to the hard core, the 1D scattering problem has the same boundary condition as the 3D reduced radial solution.
- [61] G. E. Astrakharchik and J. Boronat, "Luttinger-liquid behavior of one-dimensional <sup>3</sup>He," *Phys. Rev. B* **90**, 235439 (2014).
- [62] A. Luther and I. Peschel, "Single-particle states, Kohn anomaly, and pairing fluctuations in one dimension," *Phys. Rev. B* **9**, 2911–2919 (1974).
- [63] A. H. Castro Neto, H. Q. Lin, Y.-H. Chen, and J. M. P. Carmelo, "Pseudoparticle-operator description of an interacting bosonic gas," *Phys. Rev. B* **50**, 14032–14047 (1994).
- [64] G. E. Astrakharchik and L. P. Pitaevskii, "Motion of a heavy impurity through a Bose-Einstein condensate," *Phys. Rev. A* **70**, 013608 (2004).
- [65] A pioneering, but less general, fit of imaginary-time density correlations was performed for the dipolar gas in S. De Palo, E. Orignac, R. Citro, and M. L. Chiofalo, "Low-energy excitation spectrum of one-dimensional dipolar quantum gases," *Phys. Rev. B* **77**, 212101 (2008).
- [66] E. H. Lieb and W. Liniger, "Exact Analysis of an Interacting Bose Gas. I. The General Solution and the Ground State," *Phys. Rev.* **130**, 1605–1616 (1963).
- [67] E. H. Lieb, "Exact Analysis of an Interacting Bose Gas.

- II. The Excitation Spectrum,” *Phys. Rev.* **130**, 1616–1624 (1963).
- [68] M. Rossi and L. Salasnich, “Path-integral ground state and superfluid hydrodynamics of a bosonic gas of hard spheres,” *Phys. Rev. A* **88**, 053617 (2013).
- [69] R. A. Cowley and A. D. B. Woods, “Inelastic Scattering of Thermal Neutrons from Liquid Helium,” *Can. J. Phys.* **49**, 177–200 (1971).
- [70] D. E. Galli, E. Cecchetti, and L. Reatto, “Rotons and Roton Wave Packets in Superfluid  $^4\text{He}$ ,” *Phys. Rev. Lett.* **77**, 5401–5404 (1996).
- [71] We analyzed data from M. Panfil, J. De Nardis, and J.-S. Caux, “Metastable Criticality and the Super Tonks-Girardeau Gas,” *Phys. Rev. Lett.* **110**, 125302 (2013).
- [72] G. E. Astrakharchik, J. Boronat, J. Casulleras, and S. Giorgini, “Beyond the Tonks-Girardeau Gas: Strongly Correlated Regime in Quasi-One-Dimensional Bose Gases,” *Phys. Rev. Lett.* **95**, 190407 (2005).
- [73] E. Haller, M. Gustavsson, M. J. Mark, J. G. Danzl, R. Hart, G. Pupillo, and H.-C. Nägerl, “Realization of an Excited, Strongly Correlated Quantum Gas Phase,” *Science* **325**, 1224–1227 (2009).
- [74] T. Nagamiya, “Statistical Mechanics of One-dimensional Substances I,” *Proc. Phys. Math. Soc. Jpn.* **22**, 705–720 (1940).
- [75] B. Sutherland, “Quantum Many-Body Problem in One Dimension: Thermodynamics,” *J. Math. Phys.* **12**, 251–256 (1971).
- [76] M. Motta, G. Bertaina, M. Rossi, E. Vitali and D. E. Galli, in preparation.
- [77] R. G. Pereira, J. Sirker, J.-S. Caux, R. Hagemans, J. M. Maillet, S. R. White, and I. Affleck, “Dynamical Spin Structure Factor for the Anisotropic Spin-1/2 Heisenberg Chain,” *Phys. Rev. Lett.* **96**, 257202 (2006).
- [78] A. Y. Cherny, J.-S. Caux, and J Brand, “Theory of superfluidity and drag force in the one-dimensional Bose gas,” *Front. Phys.* **7**, 54–71 (2012).
- [79] A. W. Sandvik, “Constrained sampling method for analytic continuation,” arXiv:1502.06066 (2015).
- [80] Calculation of  $\lambda(q)$  at momenta slightly larger than  $2k_F$  and  $4k_F$  was prevented by the difficulty of resolving a vanishing spectrum in a narrow frequency range below the dominant higher-energy peak.
- [81] A small discrepancy is seen around  $q = k_F$  where in fact the threshold for  $^4\text{He}$  seems to be higher than that predicted by the HR model.
- [82] H. Schempp, G. Günter, M. Robert-de-Saint-Vincent, C. S. Hofmann, D. Breyel, A. Komnik, D. W. Schönleber, M. Gärtner, J. Evers, S. Whitlock, and M. Weidemüller, “Full Counting Statistics of Laser Excited Rydberg Aggregates in a One-Dimensional Geometry,” *Phys. Rev. Lett.* **112**, 013002 (2014).
- [83] P. Schauß, M. Cheneau, M. Endres, T. Fukuhara, S. Hild, A. Omran, T. Pohl, C. Gross, S. Kuhr, and I. Bloch, “Observation of spatially ordered structures in a two-dimensional Rydberg gas,” *Nature* **491**, 87–91 (2012).

# Supplemental Material: One-dimensional liquid $^4\text{He}$ : dynamical properties beyond Luttinger liquid theory

Note: citations in this Supplemental Material refer to the bibliography in the main paper.

## PATH-INTEGRAL GROUND STATE METHOD

The Path Integral Ground State (PIGS) Monte Carlo method is a projector technique that provides direct access to ground-state expectation values of bosonic systems, given the microscopic Hamiltonian  $\hat{H}$  [34]. The method is exact, within unavoidable statistical error bars, which can nevertheless be reduced by performing longer simulations, as in all Monte Carlo methods. Observables  $\hat{O}$  are calculated as  $\langle \hat{O} \rangle = \lim_{\tau \rightarrow \infty} \langle \Psi_\tau | \hat{O} | \Psi_\tau \rangle / \langle \Psi_\tau | \Psi_\tau \rangle$ , where  $\Psi_\tau = e^{-\tau \hat{H}} \Psi_T$  is the imaginary-time projection of an initial trial wave-function  $\Psi_T$ . Provided non-orthogonality to the ground state, the quality of the wave-function only influences the projection time practically involved in the limit and the variance of the results.

In our study we have employed a trial Shadow wave function (SWF) [38], which is known to provide a very accurate description of the ground state of liquid and solid  $^4\text{He}$  in higher dimensions, since it introduces high order correlations in an implicit way by means of auxiliary variables. The SWF has the form  $\Psi_T(\mathbf{R}) = \int d\mathbf{S} G(\mathbf{R}; \mathbf{S})$ , where  $\mathbf{R} = \{r_1 \dots r_N\}$  ( $\mathbf{S} = \{s_1 \dots s_N\}$ ) indicates the coordinates of the  $N$  particles (shadow auxiliary variables) and  $G(\mathbf{R}; \mathbf{S}) = \prod_{i < j} \phi_P(|r_i - r_j|) \prod_{i < j} \phi_S(|s_i - s_j|) \prod_i f_{PS}(|r_i - s_i|)$ .  $f_{PS}(r) = \exp(-Cr^2)$  is a Gaussian coupling between particle and shadow variables, while  $\phi_{P,S}(r) = \exp(-u_{P,S}(r)/2)$  are Jastrow factors. We take  $u_P(r) = (b_P/r)^{m_P}$  of the standard McMillan type, while  $u_S(r) = (b_S/r)^{m_S} - \alpha \log(\sin(\pi r/L)) \tanh(r/\bar{r})$ , where  $L$  is the size of the simulation box. The additional term in the Shadow factor is a long-range correlation of the one-dimensional Reatto-Chester form [37], introduced to ensure a more rapid convergence of long-range correlations which are relevant for Luttinger liquids. In fact  $\alpha$  can be related to the Luttinger parameter by  $\alpha = 2/K_L$ . The  $\tanh(r/\bar{r})$  factor is introduced solely to avoid perturbation of the short-range regime. All parameters in the trial wave-function are variationally optimized before projecting with the PIGS method, in order to maximize efficiency of the simulations.

In the PIGS method the imaginary time  $\tau$  of propagation is split into  $M_P$  time steps of size  $\delta\tau = \tau/M_P$  so that a suitable short-time approximation for the propagator

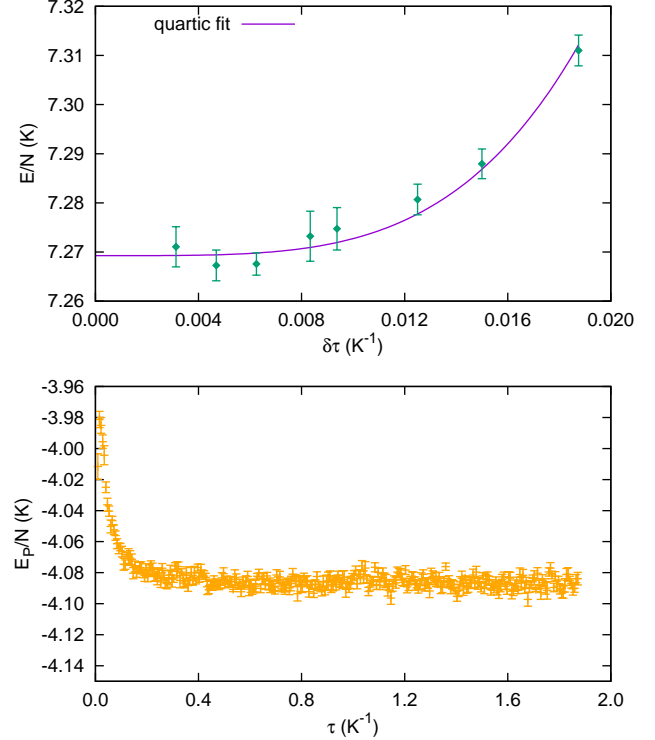


Figure S1. Upper panel: Time-step analysis of the energy per particle of  $N = 10$  atoms at the density  $\rho = 0.300\text{\AA}^{-3}$ , with a total small projection time of  $\tau = 0.075\text{K}$ . Solid line: quartic fit to the data. Lower panel: mixed potential energy of  $N = 100$  atoms at the density  $\rho = 0.300\text{\AA}^{-3}$  as a function of projection time. The corresponding variational estimate is  $E_P/N = -4.377(6)\text{K}$ .

can be used. We employ the fourth-order pair-Suzuki approximation [36] and observe convergence of ground-state estimates with a typical projection time  $\tau \simeq 0.8\text{K}^{-1}$  using a time step  $\delta\tau = 1/160\text{K}^{-1}$  (See Fig. S1 for typical time-step and total-time analyses). Once convergence is obtained, a further projection time of typical duration  $\tau_F = M\delta\tau \simeq 2\text{K}^{-1}$  is used to sample the intermediate scattering function  $F(q, \tau)$  (Eq. 4 in main text). This projection time allows us to resolve the main features of the density fluctuations spectrum and, in the high-density regime, to quantitatively extract information on the spectral shape at low-energy.



$\rho = 0.300\text{\AA}^{-1}$			$\rho = 0.220\text{\AA}^{-1}$		
N	$\mathcal{E}_N [K]$	$\sigma_N [K]$	N	$\mathcal{E}_N [K]$	$\sigma_N [K]$
10	7.26	0.01	10	0.658	0.003
20	7.37	0.01	20	0.673	0.002
30	7.37	0.01	30	0.679	0.002
40	7.41	0.01	40	0.679	0.002
50	7.40	0.008	80	0.679	0.002
80	7.41	0.008	160	0.682	0.002
100	7.41	0.008			
160	7.41	0.009			

Table I. Equation of state at high density.

### FINITE-SIZE EFFECTS

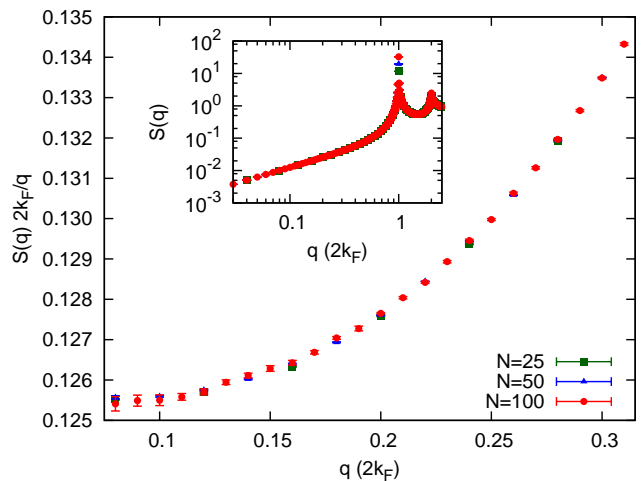
The vast majority of QMC methods give access to the properties of finite systems, made of  $N$  particles enclosed in a spatial region of volume  $V$ . However, we are interested in the properties of the system in the limit  $N \rightarrow \infty$  keeping the density  $\rho \equiv \frac{N}{V}$  fixed. We therefore must assess for which size results are compatible with those at the thermodynamic limit within the statistical uncertainties of the simulation.

In this Section, we present and describe the size effects on the equation of state, static structure factor and imaginary-time correlation functions of up to 160 Helium atoms at the highest density  $\rho = 0.300\text{\AA}^{-1}$  to show that, except in special circumstances, results for a system of  $N = 50$  Helium atoms are representative of the thermodynamic limit. Nonetheless, static properties presented in this work have been calculated using up to  $N = 160$  particles.

#### Equation of state

In Table I we report the ground-state energy per particle  $\mathcal{E}_N$  as a function of the number of atoms, at the density  $\rho = 0.300\text{\AA}^{-1}$ . The dependence of the results on  $N$  is well captured by the formula  $\mathcal{E}_N = e_1 + \frac{e_2}{N^2}$  with  $e_1 = 7.408(5) K$ . This functional form reveals that size-effects on the equation of state are modest, in that the ground-state energies of 40 or more atoms are compatible with each other and with  $e_1$ . The expression of  $\mathcal{E}_N$  also reflects the similarity between Helium atoms in the high-density regime and hard rods: indeed, for the HR system, the relation  $\mathcal{E}_N = e_1 (1 - \frac{1}{N^2})$  holds exactly [5]. For a more detailed comparison, we also report the ground-state energy per particle of systems at  $\rho = 0.220\text{\AA}^{-1}$ . For  $N \geq 30$ , results are compatible with each other within the statistical uncertainties of the simulations, around 2%.

At lower densities, size effects on the equation of state are even more modest, implying that the ground-state energies of 20 or more atoms are compatible with each

Figure S2. Static structure factor at  $\rho = 0.220\text{\AA}^{-1}$  for various systems sizes (inset), divided by  $q/2k_F$  at low momenta (main figure).

other. It is worth recalling that  $K_L$  can be estimated from the equation of state by fitting the latter to a polynomial in the density and computing  $K_L$  as function of the fitting parameters. Such procedure, however, involves error propagation from the fitting parameters to the estimator of  $K_L$ . At low density, this is responsible for the large error bars in the estimates of  $K_L$  in Fig. 1 of the main text.

#### Static structure factor

In Fig. S2 we show the ratio  $2k_F S(q)/q$ , for systems of  $N = 25, 50$  and  $100$  atoms at the highest density. This quantity has been used to estimate the Luttinger parameter, taking advantage of the relation  $S(q) \sim K_L \frac{q}{2k_F}$ , holding in the low-momentum regime. Using results for  $N = 50$  particles, we obtain  $K_L = 0.1255(5)$ . This result is compatible with that obtained for  $N = 100$  particles, confirming the robustness and the absence of size effects of our estimate for  $K_L$ .

Away from a narrow neighborhood of the Umklapp points  $q_j = 2j k_F$ , with  $j$  integer, results for  $S(q)$  relative to  $N = 50, 100$  particles are compatible with each other within the statistical uncertainties of the calculations, which in all cases are well below 1%. The presence of peaks diverging with the system size limits the possibility of producing estimates of  $S(q_n)$ ,  $S(q_n, \omega)$  free from size effects. However, away from the Umklapp points, estimates of  $S(q)$  for  $N = 50$  particles are representative of the thermodynamic limit.

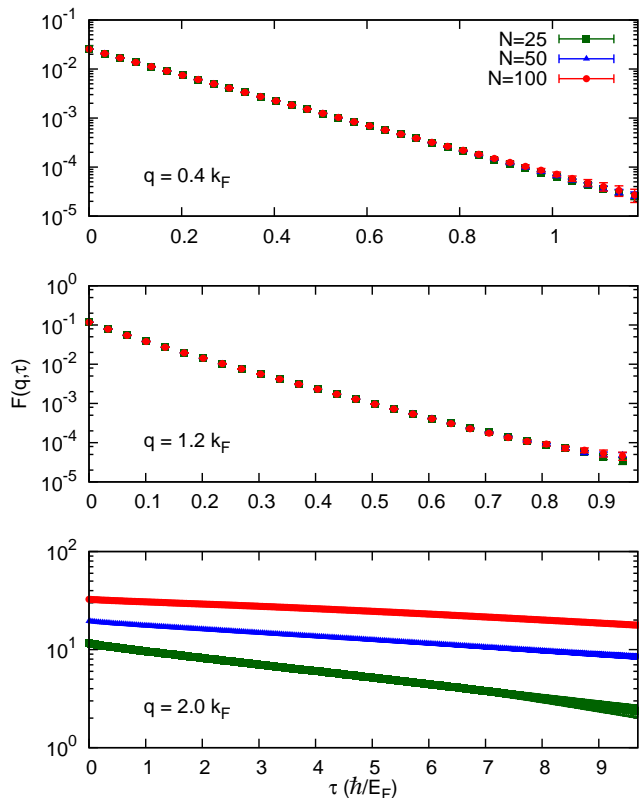


Figure S3. (color online) Imaginary-time density-density correlation function  $F(q, \tau)$  at  $\rho = 0.300 \text{ \AA}^{-1}$  for various systems sizes at three representative momenta.

### Imaginary-time correlation functions

Given the limited size effects observed in the static structure factor, and the central role of  $S(q, \omega)$  in the present work, it is very important to investigate the size effects on the imaginary-time correlation functions. We illustrate  $F(q, \tau)$  in Fig. S3 for systems of  $N = 25, 50, 100$  particles at the highest density  $\rho = 0.300 \text{ \AA}^{-1}$ , for the wavevectors  $q/k_F = 0.4, 1.2, 2$ , representative of the low-momentum, intermediate-momentum and Umklapp regimes. Size effects on imaginary-time correlation functions agree with those in the static structure factor. In particular strong effects are seen only around the Umklapp points.

The analysis of the high-imaginary time region reveals that a precise determination of the low-energy threshold  $\omega_{\text{th}}(q)$  is made difficult by the growth of relative errors with imaginary time, more than by size effects. The uncertainty on the low-energy threshold naturally has a negative impact on the possibility of assessing a power-law behavior of  $S(q, \omega)$  close to  $\omega_{\text{th}}(q)$ . Therefore, in order to produce a quantitative estimate of the exponents of the nonlinear-TLL theory as presented in the main text, we employed analytical information for an equivalent hard

rods system as described in the following Sections.

### GENETIC INVERSION VIA FALSIFICATION OF THEORIES METHOD

Eq. (4) in the main text is a Fredholm equation of the first kind and is an ill-conditioned problem, because a small variation in the imaginary-time intermediate scattering function  $F$  produces a large variation in the dynamical structure factor  $S$ . At fixed momentum  $q$ , the computed values  $F_j = F(q, j\delta\tau)$ , where  $j = 0 \dots M$ , are inherently affected by statistical uncertainties  $\delta F_j$ , which hinder the possibility of deterministically infer a single  $S(q, \omega)$ , without any other assumption on the solution. The Genetic Inversion via Falsification of Theories method (GIFT) exploits the information contained in the uncertainties to randomly generate  $Q$  compatible instances of the scattering function  $F^{(z)}$ , with  $z = 1 \dots Q$ , which are independently analyzed to infer  $Q$  corresponding spectra  $S^{(z)}$ , whose *average* is taken to be the “solution”. This averaging procedure, which typifies the class of stochastic search methods [40-42], yields more accurate estimates of the spectral function than standard Maximum Entropy techniques. Although any numerical analytic continuation method, included the GIFT method, is not able to precisely resolve multiple narrow peaks if they are present, apart from the lowest energy one, the most relevant features of the spectrum are retrieved in their position and (integrated) weight. In this work we show that with GIFT even some properties of the shape of the spectra close to the lowest threshold can be reliably inferred, once quite heavy reconstructions are performed.

Given an instance  $z$ , the procedure of analytic continuation from  $F^{(z)}$  to  $S^{(z)}$  relies on a stochastic genetic evolution of a population of spectral functions of the generic type  $S^{(z)}(q, \omega) = c_0 \sum_{i=1}^{N_\omega} s_i \delta(\omega - \omega_i)$ , where  $c_0 = F^{(z)}(q, 0)$  and the zeroth momentum sum rule  $\sum_{i=1}^{N_\omega} s_i = 1$  holds. The  $N_\omega$  support frequencies  $\omega_i = \omega_{\text{th}} + \Delta\omega(i - 1/2)$  are spaced by a small  $\Delta\omega$  and a minimum threshold frequency  $\omega_{\text{th}}$  can be imposed. Genetic algorithms provide an extremely efficient tool to explore a sample space by a non-local stochastic dynamics, via a survival-to-compatibility evolutionary process mimicking the natural selection rules; such evolution aims toward increasing the *fitness* of the individuals, defined as

$$\Phi^{(z)}(S) = - \sum_{j=0}^M \frac{1}{\delta F_j^2} \left[ F_j^{(z)} - c_0 \sum_{i=1}^{N_\omega} e^{-j\delta\tau\omega_i} s_i \right]^2 - \gamma \left[ c_1 - c_0 \sum_{i=1}^{N_\omega} \omega_i s_i \right]^2, \quad (\text{S1})$$

where the first contribution favors adherence to the data, while the second one favors the fulfillment of the f-sum

rule, with  $c_1 = \frac{\hbar q^2}{2m}$  and  $\gamma$  a parameter to be tuned for efficiency. A step in the genetic evolution replaces the population of spectral functions with a new generation, by means of the “biological-like” processes of *selection*, *crossover* and *mutation*, which are described in detail in [43]. In this work we have added a *smoothing mutation*, which operates randomly on very small portions of the spectrum, and a *long-range mutation* which exchanges weight between two randomly separated bins. Moreover, the genetic evolution is tempered by an acceptance/rejection step based on a reference distribution  $p^{(z)}(S) = \exp(\Phi^{(z)}(S)/T)$ , where the coefficient  $T$  is used as an effective temperature in a standard simulated annealing procedure [40]. We found that this combination is optimal in that it combines the speed of the genetic algorithm with the prevention of strong mutation-biases thanks to the simulated annealing. Convergence is reached once  $|\Phi^{(z)}(S)| < 1$ , and the best individual, in the sense that it does not falsify the theory represented by (S1), is chosen as the representative  $S^{(z)}$ . The final spectrum, as in Fig. 3 of the main text (where no threshold is assumed), is obtained by taking the average over instances  $\bar{S}(q, \omega) = \frac{1}{Q} \sum_{z=1}^Q S^{(z)}(q, \omega)$ .

Note that the space of spectral functions that we consider is quite general, and can be extended by using smaller frequency spacing  $\Delta\omega$ . However, the purpose of GIFT is not to exactly resolve the spectrum of a finite system, which would be indeed consisting of a sum of delta-functions, but to provide a convolution, which, as such, is suited to study the thermodynamic limit. The proper quantity to be analyzed to define such limit is in fact  $F(q, \tau)$ , whose size effects we have described in the previous Section.

*Dynamical Structure Factor at specific momenta.* In Fig. S4 we show some reconstructed spectra at specific momenta, with the aim of highlighting the appearance of regions of almost flat spectral weight, either at  $q = 2k_F$  for small  $\omega$  when  $K_L \simeq 1$ , or around the special  $Q_1 = 2\pi/a$  at high density. In particular curve (a) corresponds to density  $\rho = 0.150\text{\AA}^{-1}$ , for which  $K_L \simeq 0.98$ . Data are shown above the minimal frequency corresponding to the super-current state  $\hbar\omega = (2\hbar k_F)^2/2mN$ . The comparison to the TLL prediction  $S(2k_F, \omega) \propto \omega^{2(K_L-1)}$  [62-64] (solid line) is quite satisfactory. Curves (b-d) show the spectra at the density  $\rho = 0.300\text{\AA}^{-1}$  around  $q = 3.24k_F = 3.05\text{\AA}^{-1}$ , which is the momentum displaying maximally flat spectrum in our reconstruction. The spectra shown in Fig. S4 are representative of the data used to produce Fig. 3 in the main text, where no threshold is assumed. More sophisticated and accurate continuations are used to produce Fig. 4 in the main text, with the procedure described in the next section.

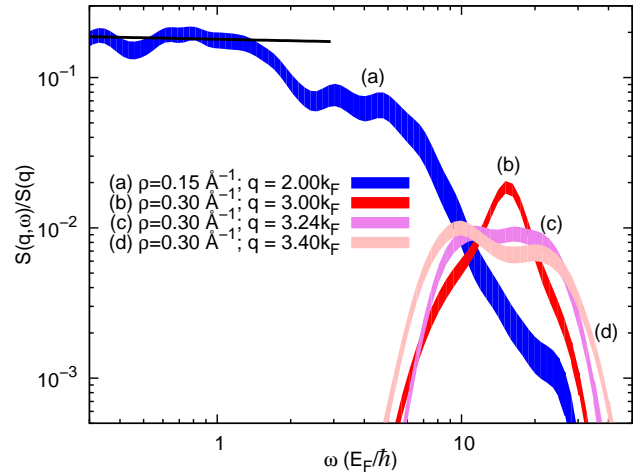


Figure S4.  $S(q, \omega)$  as a function of frequency for different momenta and densities, divided by the corresponding  $S(q)$ . Data are post-processed with a smoothing operation, while the width indicates the typical variance of reconstructions. Solid line: see text.

#### POWER-LAW FIT OF THE RECONSTRUCTED SPECTRA

We now describe with some detail the procedure employed to obtain the results presented in Fig. 4 of the main text.

In order to remove noise, we assume that the spectral weight is zero below the threshold of a system of  $N = 50$  Hard-Rods whose radius is fixed so as to have the same  $K_L = 0.1255$  as for our  $^4\text{He}$  system at the density  $\rho = 0.3\text{\AA}^{-1}$ . This is the only additional knowledge about  $S(q, \omega)$  enforced in our reconstruction. We take advantage of the following analytical expression for the threshold of a system of  $N$  hard rods:

$$\omega_{\text{th}}^{(N)}(q) = \omega_{\text{th}}(q) \left( 1 + \frac{1}{N} \right) + \omega_{\text{sc}}(q), \quad (\text{S2})$$

where the threshold in the thermodynamic limit is  $\omega_{\text{th}}(q) = \omega^-(q - 2nk_F)/K_L$  with  $2nk_F < q < 2(n+1)k_F$  and  $n$  integer, as described in the main text, while two corrections have to be added for finite systems:  $\omega_{\text{th}}(q)/N$  and  $\omega_{\text{sc}}(q) = \frac{\hbar q^2}{2mN}$ , corresponding to the energy of a super-current state [76]. When the threshold cannot be reasonably assumed, a general method has been recently proposed [79]. In the future, it would be interesting to investigate whether such method can yield reliable threshold energies in the intermediate-to-low-energy regime.

For each momentum, we then exploit the imaginary-time correlation functions  $F(q, \tau)$  obtained with the PIGS simulations, with their statistical error bars, to sample  $Q = 1280$  compatible  $F^{(z)}$ . Instead of taking a single average, as in the previous section, the  $Q$  reconstructed spectra are averaged over blocks of 128 elements,

yielding  $B = 10$  estimated spectra, which are fitted with the following expression:

$$S_i = A(\omega_i - \omega_{\text{th}})^{-\mu} Q_i, \quad (\text{S3})$$

where  $Q_i = \frac{\tilde{\omega}_i}{(1-\mu)} \left[ \left(1 + \frac{1}{2\tilde{\omega}_i}\right)^{1-\mu} - \left(1 - \frac{1}{2\tilde{\omega}_i}\right)^{1-\mu} \right]$  with  $\tilde{\omega}_i = (\omega_i - \omega_{\text{th}})/\Delta\omega$ . This expression is the average value of the power-law model in the interval  $[\omega_i - \Delta\omega/2, \omega_i + \Delta\omega/2]$ , and it is the correct way to compare our discrete-frequency spectra to the model, especially close to  $\omega_{\text{th}}$  when a divergence is expected. The range of the fitting procedure is from  $\omega = \omega_{\text{th}}$  to the maximum frequency yielding a reduced Chi-square  $\chi^2/\nu \simeq 1$ . Such maximum frequency for a best fit depends on  $q$  but it is typically of order  $q \approx 0.3k_F$ . Each of the  $B$  fits yields a value for  $\mu$ , the mean value and standard deviation of which are showed in Fig. 4 of the main text. In Fig S5 we show some of the averaged spectra at different momenta together with Eq. (S3) using the mean of  $A$  and  $\mu$ . In panel (d) one can see that the first frequency bin is not well fitted by the power-law model. This is typical of the spectra where the spectral weight decreases towards the threshold. The effect is much more pronounced for the momenta close but higher than multiples of  $2k_F$ , which has prevented us to extract reliable exponents in such cases. We cannot assess whether this indicates a truly finite spectral weight, beyond the power-law model, or, more probably, an unavoidable limitation of analytical continuation strategies. However, for negative values of the exponent, giving rise to a divergence in the spectrum at  $\omega = \omega_{\text{th}}(q)$ , our procedure has provided robust evidence of a power-law singularity in the dynamical structure factor consistent with the HR model.

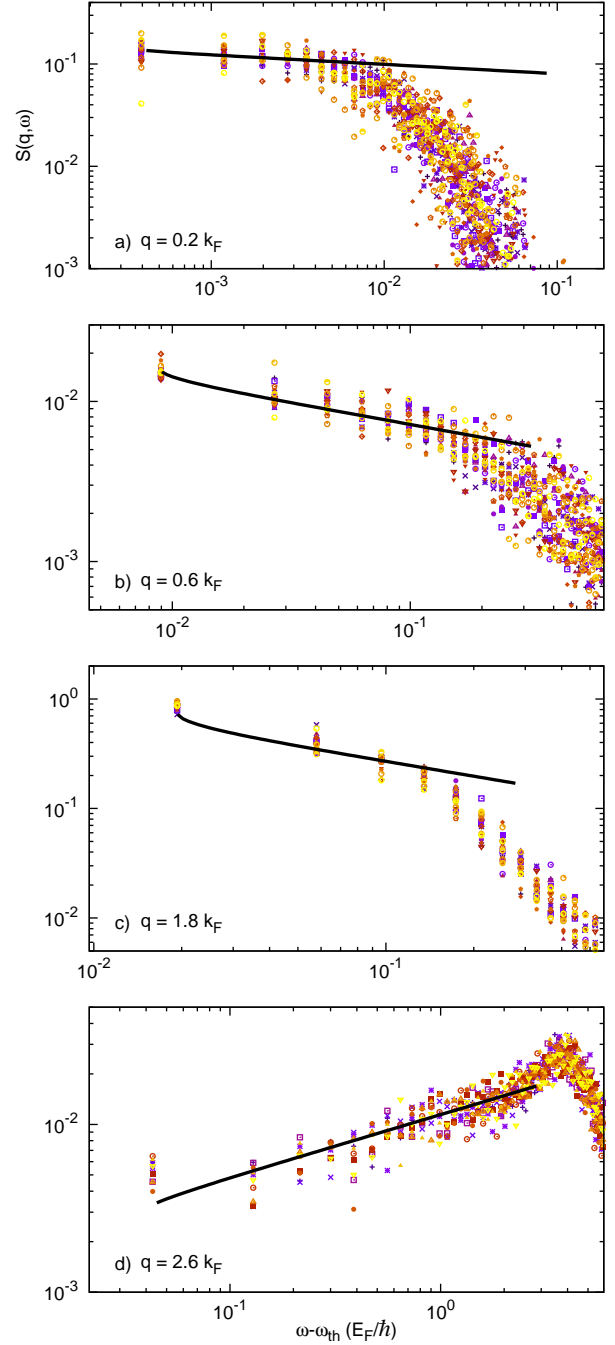


Figure S5. Set of block averages of the dynamical structure factor reconstructed at  $\rho = 0.300\text{\AA}^{-1}$  and various momenta. Solid lines are Eq.(S3), using the mean of  $A$  and  $\mu$  obtained from the fits of the block averaged spectra. Panel a: momentum  $q = 0.2k_F$  and  $\hbar\omega_{\text{th}} = 2.927E_F$ . Panel b:  $q = 0.6k_F$  and  $\hbar\omega_{\text{th}} = 6.834E_F$ . Panel c:  $q = 1.8k_F$  and  $\hbar\omega_{\text{th}} = 2.991E_F$ . Panel d:  $q = 2.6k_F$  and  $\hbar\omega_{\text{th}} = 6.962E_F$ .